Published in final edited form as:
Phys Med Biol. 2010 October 21; 55(20): 6141–6155. doi:10.1088/0031-9155/55/20/007.

In vivo transcranial cavitation threshold detection during ultrasound-induced blood–brain barrier opening in mice

Yao-Sheng Tung[1], **Fotios Vlachos**[1], **James J Choi**[1], **Thomas Deffieux**[1], **Kirsten Selert**[1], and **Elisa E Konofagou**[1,2,3]

[1]Department of Biomedical Engineering, Columbia University, New York, NY, USA

[2]Department of Radiology, Columbia University, New York, NY, USA

Abstract

The *in vivo* cavitation response associated with blood–brain barrier (BBB) opening as induced by transcranial focused ultrasound (FUS) in conjunction with microbubbles was studied in order to better identify the underlying mechanism in its noninvasive application. A cylindrically focused hydrophone, confocal with the FUS transducer, was used as a passive cavitation detector (PCD) to identify the threshold of inertial cavitation (IC) in the presence of Definity® microbubbles (mean diameter range: 1.1–3.3 μm, Lantheus Medical Imaging, MA, USA). A vessel phantom was first used to determine the reliability of the PCD prior to *in vivo* use. A cerebral blood vessel was simulated by generating a cylindrical channel of 610 μm in diameter inside a polyacrylamide gel and by saturating its volume with microbubbles. The microbubbles were sonicated through an excised mouse skull. Second, the same PCD setup was employed for *in vivo* noninvasive (i.e. transdermal and transcranial) cavitation detection during BBB opening. After the intravenous administration of Definity® microbubbles, pulsed FUS was applied (frequency: 1.525 or 1.5 MHz, peak-rarefactional pressure: 0.15–0.60 MPa, duty cycle: 20%, PRF: 10 Hz, duration: 1 min with a 30 s interval) to the right hippocampus of twenty-six (n = 26) mice *in vivo* through intact scalp and skull. T1 and T2-weighted MR images were used to verify the BBB opening. A spectrogram was generated at each pressure in order to detect the IC onset and duration. The threshold of BBB opening was found to be at a 0.30 MPa peak-rarefactional pressure *in vivo.* Both the phantom and *in vivo* studies indicated that the IC pressure threshold had a peak-rarefactional amplitude of 0.45 MPa. This indicated that BBB opening may not require IC at or near the threshold. Histological analysis showed that BBB opening could be induced without any cellular damage at 0.30 and 0.45 MPa. In conclusion, the cavitation response could be detected without craniotomy in mice and IC may not be required for BBB opening at relatively low pressures.

1. Introduction

The central nervous system (CNS) has been shown to pose a formidable challenge in drug delivery. The blood–brain barrier (BBB) prevents most neurological drugs from traversing from the cerebral microvasculature into the brain parenchyma. Out of all the methods

[3]Author to whom any correspondence should be addressed. ek2191@columbia.edu.

available for BBB opening (Pardridge 2010), focused ultrasound (FUS) combined with microbubbles has been validated as the only technique aside from chemical and biological methods to noninvasively and locally open the BBB (Choi *et al* 2007a, Hynynen *et al* 2001, McDannold *et al* 2005). Albeit the minute target involved, the mouse serves as a good animal model for transcranial BBB opening investigation as well as acoustic emission detection because of its thinner skull (Tung *et al* 2010). In larger animals such as rabbits (Hynynen *et al* 2001), rats (Liu *et al* 2008) and pigs (Xie *et al* 2008), craniotomy is typically required because of large phase aberrations produced by skulls of larger animals (Hynynen *et al* 2001, McDannold *et al* 2005, 2006, 2007). Our group has reported localized BBB opening through the intact scalp and skull in wild-type mice (Choi *et al* 2007a, 2007b), in an Alzheimer's disease (AD) mouse model (Choi *et al* 2008), and has quantified the extents of BBB opening using variable-sized dextran (Choi *et al* 2010b). The pressure threshold of BBB opening with mono-dispersed microbubbles has also been investigated (Choi *et al* 2010a). The effect of the murine skull on the inertial cavitation threshold has been investigated (Tung *et al* 2010) but the transcranial *in vivo* cavitation detection remains unexplored.

As of now, the physical mechanism responsible for the ultrasound-induced BBB opening requires complete understanding. Possible mechanisms for BBB opening via FUS and microbubbles include (1) inertial cavitation, caused by bubble collapse, that releases high energy and generates high temperatures, high pressures and/or high-velocity jets, which may damage the surrounding tissue (Miller *et al* 1996, Crum 1988); (2) stable cavitation, bubble oscillation and microstreaming (Nyborg 2001) surrounding the microbubbles that may induce shear stresses affecting the tight junctions; or (3) ischemia caused by bubble expansions, which may reduce the blood flow transiently (Chen *et al* 2009).

When microbubbles are confined within a vessel, the bubble behavior changes due to the vessel wall constraints. Some numerical studies have predicted how the vessel size and stiffness affect the bubble behavior. In rigid vessels, it has been shown that the resonance frequency of microbubbles decrease as the vessel diameter decreases (Sassaroli and Hynynen 2005). The resonance frequency of microbubbles also increases as the vessel compliance increases (Martynov *et al* 2009, Qin and Ferrara 2007). Because the bubble can be allowed to expand further within a compliant vessel, the threshold of bubble fragmentation, induced by the larger amplitude oscillation, decreases as the vessel compliance increases (Qin and Ferrara 2006). In simulations, the temperature rise near microbubbles within a capillary network during sonication remained below 2 °C with the 3 μm microbubbles at 1 MPa, 1 MHz and 0.5 ms sonication duration (Klotz *et al* 2010).

Rigid bubble motion, as a result of the radiation force as well as visualization of radial oscillations, has been proposed to explain why microbubbles within smaller tubes have a higher fragmentation threshold and greater persistence (Zheng *et al* 2007). The relationship between the threshold of fragmentation of ultrasonic contrast agents and the acoustic parameters used has also been investigated (Chomas *et al* 2001). However, cellulose tubes, which have been used in most vessel phantom studies, do not have the same properties as physiologic vessels. The observation of microbubble interaction with the microvessel wall of the *ex vivo* cecum has been investigated to demonstrate the process of bubble collapse

into the endothelium and repeated expansion of the microbubble within the blood vessels (Caskey *et al* 2007).

A passive cavitation detector (PCD), which can acquire acoustic emission (Roy *et al* 1985), has been used for some *in vivo* studies. It has been shown that the inertial cavitation can be correlated with cell damage in rabbit ear vessels (Hwang *et al* 2006, Tu *et al* 2006). The interaction between ultrasound and microbubbles has been shown to increase the permeability of the endothelial layer without any cell detachment or damage *in vitro* (Kooiman *et al* 2010). In order to understand the bubble behavior during BBB opening, the relationship between acoustic cavitation and BBB disruption was previously investigated using a PCD, which suggested that inertial cavitation might not be necessary for BBB opening (McDannold *et al* 2006). However, that study was performed following craniotomy. As a result, *in vivo* transcranial cavitation detection during BBB opening is necessary for understanding the actual mechanism of BBB opening induced by FUS and microbubbles without craniotomy.

The objective of this paper is to unveil the physical mechanism of transcranial BBB opening *in vivo*. First, a phantom study was carried out to separately assess the effect of the skull, the angle dependence, sensitivity and reliability of the PCD setup. The occurrence of inertial cavitation during BBB opening in mice *in vivo* was then investigated using the same PCD setup. The spectrogram and inertial cavitation dose (ICD) were used to identify the threshold of inertial cavitation. MRI and histology were respectively used to determine the BBB opening occurrence and macroscopic damage.

2. Materials and methods

2.1. Ultrasound equipment

In order to determine the sensitivity and reliability of the PCD, a vessel phantom was used. The experimental setup and procedure for the phantom study have been detailed in a previously reported study (Tung *et al* 2010). Five renditions were performed at each pressure in the phantom study. The experimental setup of *in vivo* transcranial cavitation detection is shown in figure 1. All procedures used on the mice were approved by the Columbia University Institutional Animal Care and Use Committee. Twenty-six (n = 26) adult male mice (strain: C57BL/6, weight: 26.1 ± 1.7 g, Harlan Sprague Dawley, Indianapolis, IN, USA) were sonicated. The number of mice studied at each pressure are shown in table 1. The animals were anesthetized with a mixture of oxygen (0.8 L min^{-1} at 1.0 Bar, 21 °C) and 1.5–2.0% vaporized isoflurane (Aerrane, Baxter Healthcare Corporation, Deerfield, IL) using an anesthesia vaporizer (SurgiVet, Inc., Waukesha, WI). In this study, a grid system to localize the sutures of the murine skull was used for the targeting procedure (Choi *et al* 2007a). The right hippocampus was targeted and the PCD was thus placed on the side of the right hemisphere. The focus was placed 3 mm beneath the skull so that the focal region overlapped with the right hippocampus and a small portion of the thalamus of the murine brain.

In order to maintain the stability of the microbubbles, a new vial of Definity® microbubbles (mean diameter range: 1.1–3.3 μm, Lantheus Medical Imaging, MA, USA) was activated

each time using the manufacturer's instructions and only used for the experiments within 24 h after activation. Following activation, a 1:20 dilution solution was prepared using 1× phosphate-buffered saline (PBS) and slowly injected into the tail vein (1 μL per gram of mouse body weight). Two different FUS transducers were used in this study in order to confirm that the FUS-induced BBB opening was transducer independent. The first FUS transducer (transducer-A, center frequency: 1.5 MHz; focal depth: 90 mm; outer radius: 30 mm; inner radius: 11.2 mm, Riverside Research Institute, New York, NY, USA) was the same as in the phantom study and the targeted right hippocampus was sonicated one minute after bubble injection. The second FUS transducer (transducer-B, center frequency: 1.5 MHz; focal depth: 60 mm; outer radius: 30 mm; inner radius: 11.2 mm; model: cdc7411–3, Imasonic, Besançon, France) was used to perform sonication immediately following bubble administration with the same acoustic parameters as transducer-A. A single-element, pulse-echo (P/E) diagnostic transducer (center frequency: 10 MHz, Olympus NDT, Waltham, MA, USA) with a focal length of 60 mm was positioned through the center hole of the FUS transducer so that the foci of the two transducers could be properly aligned.

Both transducers used pulsed-wave FUS (burst rate: 10 Hz; burst duration: 20 ms; duty cycle: 20%) in two 30 s sonication intervals with a 30 s intermittent delay. Peak-rarefactional acoustic pressures of 0.15, 0.30, 0.45 and 0.60 MPa were used in this study. For both transducers, these values were obtained experimentally in degassed water and adjusted to account for murine skull attenuation values of 18.1%. The left hippocampus was not targeted and was used as the control for MRI examination. The sonication on the right hippocampus without microbubbles could provide the baseline of acoustic emission acquired by the PCD. It was shown that the sonication without microbubbles at lower pressures (<2 MPa, peak-rarefactional) would not induce BBB opening (Choi *et al* 2007a). As a result, the net bubble response could be calculated after subtraction from the baseline.

2.2. Magnetic resonance imaging

A vertical-bore 9.4T MR system (Bruker Biospin, Billerica, MA, USA) was used to confirm the BBB opening in the murine hippocampus. Each mouse was anesthetized using 1–2% of isoflurane gas and was positioned inside a single resonator. The respiration rate was monitored throughout the procedure using a monitoring system (SA Instruments Inc., Stony Brook, New York, USA). Prior to introducing the mouse into the scanner, intraperitoneal (IP) catheterization was performed. Because the MR system underwent a software upgrade during the course of the study, two different protocols were used for MR imaging. The first protocol was a three-dimensional (3D), T1-weighted SNAP gradient echo pulse sequence, which acquired horizontal images using TR/TE = 20/4 ms, a flip angle of 25°, number of excitations (NEX) of 5, a total acquisition time of 6 min and 49 s, a matrix size of 256 × 256 × 16 pixels and a field of view (FOV) of 1.92 × 1.92 × 0.5 cm^3, resulting in a resolution of 75 × 75 × 312.5 μm^3. The second protocol was a 3D T2*-weighted gradient echo flow compensated (GEFC) gradient echo pulse sequence, which acquired horizontal images using TR/TE = 20/5.2 ms, a flip angle of 10°, NEX of 8, a total acquisition time of 8 min and 12 s, a matrix size of 256 × 192 × 16 pixels and a FOV of 2.25 × 1.69 × 0.7 cm^3, resulting in a resolution of 88 × 88 × 437.5 μm^3. Both protocols were applied approximately 30 min after an IP injection of 0.30 ml of gadodiamide (Omniscan®, GE Healthcare, Princeton, NJ,

USA), which allowed sufficient time for the gadodiamide to diffuse into the sonicated region.

2.3. Histology and imaging

Five hours after sonication, the mouse was euthanized and transcardially perfused with 30 mL PBS and 60 mL 4% paraformaldehyde. After soaking the brain in paraformaldehyde for 24 h, the skull was removed and the brain was fixed again in 4% paraformaldehyde for 6 days. The post-fixation processing of the brain tissue was then performed according to standard histological procedures. The paraffin-embedded specimen was sectioned horizontally at a 6-μm thick section. A 1.2-mm layer from the top of the brain was first trimmed away. A total of 12 separate levels that covered the entire hippocampus were then obtained at 80-μm intervals. At each level, six sections were acquired and the first two sections were stained with hematoxylin and eosin (H&E).

2.4. Acoustic emission signal acquisition and analysis

The acoustic emission signals acquired by the PCD were sampled at 80 MHz in the phantom study and 25 MHz in the *in vivo* study to accommodate the highest memory limit of the digitizer involved in each case. A shorter pulse length, i.e. of 100 cycles, was used in the phantom study and a longer pulse length, i.e. 30 400 cycles, as in our previous work, was used *in vivo*. A customized spectrogram function (30 cycles, i.e. 20 μs, Chebyshev window; 95% overlap; 4096-point FFT) in MATLAB® (2007b, Mathworks, Natick, MA) was used to generate a time–frequency map, which provided the spectral amplitude in time (figure 2(a)). The spectrogram can then clearly indicate how the frequency content of a signal changes over time. Therefore, the onset of the broadband response and its duration could be clearly demonstrated on the spectrogram.

In this study, the acoustic emission was quantified *in vivo*. A high-pass, Chebyshev type 1, filter with a cutoff of 4 MHz was first applied to the acquired PCD signal. The acoustic emission collected by the focused hydrophone was used in the quantification of the ICD, the harmonic (nf, n = 1, 2, . . ., 6), sub-harmonic (f/2) and ultra-harmonic (nf/2, n = 3, 5, 7, 9) frequencies produced by stable cavitation (Farny *et al* 2009) were filtered out by excluding 300 kHz bandwidths around each harmonic and 100 kHz bandwidths around each sub- and ultra-harmonic frequency. These bandwidths were designed to filter for the broadband response and to ensure that the stable cavitation response was not included in the ICD calculation. The root mean square (RMS) of the spectral amplitude (V_{RMS}) could then be obtained from the spectrogram after filtering (figure 2). Figure 2(a) depicts the spectrogram after high-pass filtering with a 4 MHz cutoff and figure 2(b) shows the corresponding V_{RMS}. To maximize the broadband response compared to the sonication without microbubbles, only 50 μs of sonication (from 0.095 ms to 0.145 ms, denoted by the two dashed lines in figure 2(b)) was considered in the ICD calculation, which was performed by integrating the V_{RMS} variation within an interval of 0.75 μs (i.e. calculating the area under the V_{RMS} curve between 0.095 ms and 0.145 ms). In order to remove the effect of the skull in the ICD calculation, the V_{RMS} in the case without microbubbles was also calculated and was subtracted from the results with the microbubbles to obtain the net bubble response. A Student's t-test was used to determine whether the ICD was statistically different between

different pressure amplitudes. A P value of $P < 0.05$ was considered to denote a significant difference in all comparisons.

3. Results

3.1. Phantom study

The frequency response of the first pulse as recorded by the 60°-PCD and 90°-PCD configurations in the presence of the skull in the wave propagation path is depicted in figure 3. Figure 3 shows that the pressure threshold of the broadband response (or, inertial cavitation) was the same between these two PCD configurations, i.e. 0.45 MPa. This indicated that the pressure threshold of the broadband response was not affected by the skull *in vivo*. At 0.30 MPa, however, the 90°-PCD could detect the ultra-harmonics but the 60°-PCD could not, which indicated that the stable cavitation response was filtered by the skull. Also, the comparison of the results between the 60°-PCD and 90°-PCD configurations showed that the second harmonic would be detected by the 60°-PCD in the absence of microbubbles at 0.30 MPa and the acoustic emission amplitude was influenced by the presence of the skull, i.e. the response was partially absorbed by the skull. At 0.45 MPa and beyond, along with the broadband emissions, both the sub- and ultra-harmonics are detected in both the 60°- and 90°-PCD cases, indicating the occurrence of stable cavitation.

3.2. In vivo transcranial cavitation detection

The confirmation of BBB opening by MRI *in vivo* and the corresponding spectrogram are depicted in figure 4 for transducer-A and in figure 5 for transducer-B. As a result of the deposition of gadodiamide into the brain parenchyma through the BBB opening, the MRI indicated that the threshold of BBB opening was at 0.30 MPa (figures 4(a) and 5(a)), but the spectrogram showed that the broadband response occurred at 0.45 MPa (figures 4(b) and 5(b),(c)). Only the first 50 μs of sonication, i.e. the duration of the broadband response from 0.095 ms to 0.145 ms, are depicted on the spectrogram (figures 4(b), (c) and 5(b),(c)). Only the first and the second harmonics were detected without microbubbles (figure 4(c)), which was consistent with the phantom study (figure 3). After bubble administration, however, higher harmonics could be detected, including the third harmonic at 0.15 MPa in the absence of BBB opening, the third to fifth harmonics at 0.30 MPa with BBB opening, and the third to eighth harmonics together with the broadband response and BBB opening at 0.45 MPa and 0.60 MPa. Unlike the skull-phantom case (figure 3), no clear sub- or ultra-harmonics were detected at or beyond 0.45 MPa, indicating possible skull aberration and microbubble flow effect *in vivo*. In order to validate the threshold of inertial cavitation during BBB opening, the 10 MHz P/E transducer was used as an additional PCD for transducer-B (figure 5(c)). The threshold of inertial cavitation was consistent between the two PCDs (figures 5(b) and (c)) and the duration of the broadband response was around 5 μs at 0.45 MPa. However, the duration of the broadband response detected from the 10 MHz P/E transducer at 0.60 MPa was 0.5 ms longer than that of the hydrophone, especially at higher frequencies. At 0.30 MPa, not only the third to fifth but also the sixth to eighth harmonics could be detected by the 10 MHz P/E transducer. A clear ultra-harmonic peak between the seventh (10.5 MHz) and eighth harmonics (12 MHz) was detected as indicated in figure 5(c).

The broadband response as detected by the PCD was quantified using the ICD (figure 6). As indicated by the ICD calculations, the ICD at 0.45 MPa and 0.60 MPa was statistically higher than at 0.30 MPa and 0.15 MPa ($P < 0.05$) (figure 6(a)), which confirmed that the threshold of inertial cavitation during BBB opening was around 0.45 MPa.

The histological findings are shown in figures 7 and 8. In the cases of BBB opening at 0.30 MPa and no BBB opening at 0.15 MPa, as confirmed by the 2D-MR horizontal images, no cell damage, e.g., red blood cell (RBC) extravasations or neuronal death (Baseri *et al* 2010), was observed after histological examination (figures 7 and 8(a)–(f)). In the case of BBB opening at 0.45 MPa, no extravasations were detected in the sonicated brain regions (figures 7 and 8(j)–(l)) even though a broadband response was detected (figures 4(b) and 5(b),(c)). The brain samples sonicated at 0.60 MPa showed higher incidence of microscopic damage at multiple distinct damaged sites (figures 7 and 8(j)–(l)). The exposure pressures that resulted in RBC extravasations were those associated with the highest ICD.

4. Discussion

The presented study noninvasively detected *in vivo* acoustic emissions during the FUS-induced BBB opening and showed that BBB could be opened without inertial cavitation or cell damage. The reliability, sensitivity and transcranial capability of our PCD setup to detect acoustic emissions was validated first in a phantom (Tung *et al* 2010). Broadband emission, a signature of IC, could be detected transcranially (with the 60°-PCD configuration) and the IC threshold was identical to that at 90° PCD (non-transcranial PCD). Hence, the PCD system used in this study was deemed suitable for transcranial *in vivo* detection of inertial cavitation.

Both the phantom and *in vivo* studies indicated that the threshold of inertial cavitation during BBB opening was at the peak-negative pressure of 0.45 MPa. This was verified qualitatively and quantitatively. When the sonication was performed one minute after bubble administration, the bubble concentration in the mouse body would decrease because the increased circulation time would increase the probability of bubble disruption, dissolution, absorption and clearance. However, the threshold of the broadband response was not affected by this 1 min delay, which indicated that the variation of bubble concentration within one minute inside the capillaries of the brain did not significantly affect the threshold of inertial cavitation.

Our findings indicated that the BBB remained intact at 0.15 MPa and opened at 0.30 MPa, which was consistent with our previous work on the threshold of BBB opening as confirmed using fluorescence imaging (Baseri *et al* 2010, Choi *et al* 2010b). In addition, a broadband response was not detected at the pressure of 0.30 MPa. Our findings were in good agreement with McDannold *et al*'s findings that indicated that the BBB in rabbits after craniotomy would be intact at 0.14 MPa and open at 0.29 MPa. The threshold of the broadband response was also found to fall around 0.40 MPa in their study. On the other hand, they proposed that the second and third harmonics may be used to monitor BBB opening. However, in our study, the third harmonic could not be used to monitor BBB opening because it could still be detected at 0.15 MPa, which was shown not to induce BBB opening. Based on the results of

our phantom study, at 0.30 MPa, the ultra-harmonics were effectively filtered by the skull (figure 3), which suggested that the stable cavitation might be responsible for BBB opening at 0.30 MPa *in vivo*, and that the associated ultra-harmonics could not be detected by the broadband hydrophone at that pressure, potentially due to sensitivity limitation and the skull presence (figures 4(b) and 5(b)). However, the signals from the 10 MHz P/E transducer with *in vivo* implementation (figure 5(c)) showed that not only could higher harmonics be detected at 0.30 MPa but also the ultra-harmonic at 11.25 MHz. Therefore, both transcranial phantom and *in vivo* studies showed that BBB opening might be induced by stable cavitation only, at or near the opening threshold. Stable cavitation was also detected as sub- and ultra-harmonics at 0.45 MPa and higher pressure amplitude in phantom but not *in vivo*, probably due to difference in skull and flow properties.

In the *in vivo* study, the fourth and fifth harmonics could be detected and associated with BBB opening at 0.30 MPa (figures 4(b) and 5(b)). This was also consistent with our phantom results, which indicated that the fourth and fifth harmonics were detected at 0.30 MPa by the 60° PCD configuration (figure 3). At 0.30 MPa, nonlinear oscillations may induce the fourth and fifth harmonics, and bubble expansions may lead to BBB opening. In simulations, the resonance frequency of a 1–2 μm diameter microbubble was about 4–8 MHz (Sassaroli and Hynynen 2005, Sun *et al* 2005), which included the fourth and fifth harmonics of 1.5 MHz. As a result, the fourth and fifth harmonics detected by the broadband hydrophone might serve as a reliable indicator of BBB opening.

The spectrogram used in this study could clearly elucidate the onset and duration of IC within a single FUS. In this study, the IC occurred at the beginning of sonication and the longest duration was around 50 μs as detected by the hydrophone (figure 4(b)) and 500 μs as detected by the 10 MHz P/E transducer (figure 5(c)) at 0.60 MPa. The overlap between the focal regions of the FUS and the 10 MHz P/E transducers was larger than with the broadband hydrophone, hence the longer duration of inertial cavitation detected. At 0.45 MPa, the broadband response was detected at the first but not the second pulse. However, at 0.60 MPa, a broadband response was detected in the first three pulses. A likely explanation for this may be that the pulse repetition frequency (PRF) used in this study was not low enough to allow blood reperfusion in the capillaries between pulses. Some microbubbles might be disrupted after the first pulse but not a sufficient number of microbubbles replenished the vessel within the interval of 80 ms (20% duty cycle, PRF = 10 Hz). However, harmonics could be detected at each pulse. Since the focal region of the PCD = was larger than the FUS one (inset of figure 1), the harmonics may be due to nonlinear oscillation of the microbubbles, which were around the FUS focal region but not activated at the highest pressure amplitude.

In the phantom study, the sub-harmonic was clearly detected at 0.30 MPa when the detection was performed without the skull in the PCD path, i.e. in the 90° PCD case, but it was masked by the skull at 60° PCD. In the *in vivo* study, sub-harmonics could not be detected transcranially and are thus probably filtered by the skull. Since the broadband response is more commonly associated with inertial cavitation, inertial cavitation was detected and quantified through the measurement of broadband emissions at different pressures.

The histological results in this study were consistent with existent literature that investigated the relationship between tissue damage and inertial cavitation (Hwang *et al* 2006, Samuel *et al* 2009). Some red blood cell extravasations were induced at 0.60 MPa but no extravasations could be found at 0.15, 0.30 and 0.45 MPa. Even with higher ICD estimated at 0.60 MPa, the extravasations were limited to two to three sections. However, in order to investigate more specific forms of cellular damage (i.e. apoptosis), more sensitive staining protocols, such as TUNEL, will be applied in future studies.

Standing waves might also be generated due to the long pulse lengths used in our *in vivo* study that may lead to peak pressure variations within the mouse brain. However, in this study, the threshold of inertial cavitation was identical between the phantom and *in vivo* studies, which indicated that the standing-wave effects might not be significant *in vivo*. This is in agreement with simulation findings predicting standing-wave effects intracranially in non-human and human primates (Deffieux and Konofagou 2010). Figures 4 and 7 also show that the inertial cavitation occurred at the beginning of sonication. Therefore, our results on the IC threshold may be independent of the number of cycles and thus potential standing wave effects. Of course, we might have to take into account the fact that the *in vitro* (atmospheric) and *in vivo* (i.e. capillary) pressures were not the same. However, the identical threshold of BBB opening across all mice and the phantom study strongly indicates the insignificance of the capillary pressure effect.

MRI in this study was solely used to confirm the BBB opening occurrence. MRI was performed after gadodiamide saturated the vasculature. No further quantitative MR image analysis was provided here. A quantitative MR analysis focusing on the BBB permeability after opening has been performed and provided elsewhere (Vlachos *et al* 2010).

Because the bubble response could be detected through the skull, more parameters should be investigated to unveil the mechanism of BBB opening noninvasively. The microbubbles used in this study were commercial ultrasound contrast agents, which were poly-dispersed. Because the threshold of BBB opening was shown to be higher for the 1-2 μm than for the 4-5 μm bubbles (Choi *et al* 2010a), the size-dependent threshold of inertial cavitation should be investigated to identify the role of different bubble diameters on the inertial cavitation and BBB opening. Finally, a smaller pressure step size can be used to identify a more precise IC pressure threshold associated with BBB opening by using more sensitive instrumentation.

In summary, preliminary investigation of the *in vivo* transcranial cavitation detection and quantification of the IC activity during BBB opening was presented. The bubble behavior was shown to be detectable *in vivo* through the intact scalp and skull. The threshold of inertial cavitation using transcranial FUS and microbubbles in a vessel phantom was also investigated to provide complementary information to the *in vivo* findings. We demonstrated that (1) the threshold of inertial cavitation is not influenced by the presence of the murine skull in the FUS beam path and the inertial cavitation response could be detected transcranially during BBB opening; (2) the inertial cavitation pressure threshold lay at 0.45 MPa but the BBB was opened at 0.30 MPa, i.e. BBB can be opened without requiring inertial cavitation; (3) the fourth and fifth harmonics may serve as reliable indicators for

BBB opening *in vivo*; (4) BBB could be opened without IC at 0.30 MPa or any cellular damage below 0.45 MPa.

Acknowledgments

This study was supported in part by NIH R01EB009041, NIH R21EY018505 and NSF CAREER 0644713. The authors wish to thank Keith Yeager, BS, Department of Biomedical Engineering, Columbia University, for manufacturing the hydrophone holder used in this study. They also thank Jonathan Vappou, PhD, Jianwen Luo, PhD, Wei-Ning Lee, PhD, Jean Provost, MS and Yi Hou, MS, Department of Biomedical Engineering, Columbia University, for their important input.

References

Baseri B, Choi JJ, Tung YS, Konofagou EE. Multi-modality safety assessment of blood–brain barrier opening using focused ultrasound and Definity microbubbles: a short-term study. Ultrasound Med. Biol. 2010; 36:1445–59. [PubMed: 20800172]

Caskey CF, Stieger SM, Qin S, Dayton PA, Ferrara KW. Direct observations of ultrasound microbubble contrast agent interaction with the microvessel wall. J. Acoust. Soc. Am. 2007; 122:1191–200. [PubMed: 17672665]

Chen B, Friedman B, Cheng Q, Tsai P, Schim E, Kleinfeld D, Lyden PD. Severe blood–brain barrier disruption and surrounding tissue injury. Stroke. 2009; 40:e666–74. [PubMed: 19893002]

Choi JJ, Feshitan JA, Baseri B, Wang S, Tung YS, Borden MA, Konofagou EE. Microbubble-size dependence of focused ultrasound-induced blood–brain barrier opening in mice in vivo. IEEE Trans. Biomed. Eng. 2010a; 57:145–54. [PubMed: 19846365]

Choi JJ, Pernot M, Brown TR, Small SA, Konofagou EE. Spatio-temporal analysis of molecular delivery through the blood–brain barrier using focused ultrasound. Phys. Med. Biol. 2007a; 52:5509–30. [PubMed: 17804879]

Choi JJ, Pernot M, Small SA, Konofagou EE. Noninvasive, transcranial and localized opening of the blood–brain barrier using focused ultrasound in mice. Ultrasound Med. Biol. 2007b; 33:95–104. [PubMed: 17189051]

Choi JJ, Wang S, Brown TR, Small SA, Duff KE, Konofagou EE. Noninvasive and transient blood–brain barrier opening in the hippocampus of Alzheimer's double transgenic mice using focused ultrasound. Ultrason. Imaging. 2008

Choi JJ, Wang S, Tung YS, Morrison B III, Konofagou EE. Molecules of various pharmacologically-relevant sizes can cross the ultrasound-induced blood–brain barrier opening in vivo. Ultrasound Med. Biol. 2010b; 36:58–67. [PubMed: 19900750]

Chomas JE, Dayton P, May D, Ferrara K. Threshold of fragmentation for ultrasonic contrast agents. J. Biomed. Opt. 2001; 6:141–50. [PubMed: 11375723]

Crum LA. Cavitation microjets as a contributory mechanism for renal calculi disintegration in ESWL. J. Urol. 1988; 140:1587–90. [PubMed: 3057239]

Deffieux T, Konofagou EE. Numerical study of practical transcranial-focused ultrasound applied to blood–brain barrier opening. IEEE Trans. Ultrason. Ferroelectr. Freq. control. 2010 in press.

Farny CH, Holt RG, Roy RA. Temporal and spatial detection of HIFU-induced inertial and hot-vapor cavitation with a diagnostic ultrasound system. Ultrasound Med. Biol. 2009; 35:603–15. [PubMed: 19110368]

Hwang JH, Tu J, Brayman AA, Matula TJ, Crum LA. Correlation between inertial cavitation dose and endothelial cell damage in vivo. Ultrasound Med. Biol. 2006; 32:1611–9. [PubMed: 17045882]

Hynynen K, McDannold N, Vykhodtseva N, Jolesz FA. Noninvasive MR imaging-guided focal opening of the blood–brain barrier in rabbits. Radiology. 2001; 220:640–6. [PubMed: 11526261]

Klotz AR, Lindvere L, Stefanovic B, Hynynen K. Temperature change near microbubbles within a capillary network during focused ultrasound. Phys. Med. Biol. 2010; 55:1549–61. [PubMed: 20164536]

Kooiman K, Emmer M, Foppen-Harteveld M, van Wamel A, de Jong N. Increasing the endothelial layer permeability through ultrasound-activated microbubbles. IEEE Trans. Biomed. Eng. 2010; 57:29–32. [PubMed: 19709954]

Liu HL, Wai YY, Chen WS, Chen JC, Hsu PH, Wu XY, Huang WC, Yen TC, Wang JJ. Hemorrhage detection during focused-ultrasound-induced blood–brain-barrier opening by using susceptibility-weighted magnetic resonance imaging. Ultrasound Med. Biol. 2008; 34:598–606. [PubMed: 18313204]

Martynov S, Stride E, Saffari N. The natural frequencies of microbubble oscillation in elastic vessels. J. Acoust. Soc. Am. 2009; 126:2963–72. [PubMed: 20000909]

McDannold N, Vykhodtseva N, Hynynen K. Targeted disruption of the blood–brain barrier with focused ultrasound: association with cavitation activity. Phys. Med. Biol. 2006; 51:793–807. [PubMed: 16467579]

McDannold N, Vykhodtseva N, Hynynen K. Use of ultrasound pulses combined with Definity for targeted blood–brain barrier disruption: a feasibility study. Ultrasound Med. Biol. 2007; 33:584–90. [PubMed: 17337109]

McDannold N, Vykhodtseva N, Raymond S, Jolesz FA, Hynynen K. MRI-guided targeted blood–brain barrier disruption with focused ultrasound: histological findings in rabbits. Ultrasound Med. Biol. 2005; 31:1527–37. [PubMed: 16286030]

Miller MW, Miller DL, Brayman AA. A review of in vitro bioeffects of inertial ultrasonic cavitation from a mechanistic perspective. Ultrasound Med. Biol. 1996; 22:1131–54. [PubMed: 9123638]

Nyborg WL. Biological effects of ultrasound: development of safety guidelines. Part II: general review. Ultrasound Med. Biol. 2001; 27:301–33. [PubMed: 11369117]

Pardridge WM. Biopharmaceutical drug targeting to the brain. J. Drug Target. 2010; 18:157–67. [PubMed: 20064077]

Qin S, Ferrara KW. Acoustic response of compliable microvessels containing ultrasound contrast agents. Phys. Med. Biol. 2006; 51:5065–88. [PubMed: 17019026]

Qin S, Ferrara KW. The natural frequency of nonlinear oscillation of ultrasound contrast agents in microvessels. Ultrasound Med. Biol. 2007; 33:1140–8. [PubMed: 17478030]

Roy RA, Atchley AA, Crum LA, Fowlkes JB, Reidy JJ. A precise technique for the measurement of acoustic cavitation thresholds and some preliminary results. J. Acoust. Soc. Am. 1985; 78:1799–805. [PubMed: 4067082]

Samuel S, Fowlkes JB, Miller DL. An in vitro study of the correlation between bubble distribution, acoustic emission and cell damage by contrast ultrasound. IEEE Trans. Ultrason. Ferroelectr. Freq. Control. 2009; 56:589–99. [PubMed: 19411217]

Sassaroli E, Hynynen K. Resonance frequency of microbubbles in small blood vessels: a numerical study. Phys. Med. Biol. 2005; 50:5293–305. [PubMed: 16264254]

Sun Y, Kruse DE, Dayton PA, Ferrara KW. High-frequency dynamics of ultrasound contrast agents. IEEE Trans. Ultrason. Ferroelectr. Freq. Control. 2005; 52:1981–91. [PubMed: 16422410]

Tu J, Matula TJ, Brayman AA, Crum LA. Inertial cavitation dose produced in ex vivo rabbit ear arteries with Optison by 1 MHz pulsed ultrasound. Ultrasound Med. Biol. 2006; 32:281–8. [PubMed: 16464673]

Tung YS, Choi JJ, Baseri B, Konofagou EE. Identifying the inertial cavitation threshold and skull effects in a vessel phantom using focused ultrasound and microbubbles. Ultrasound Med. Biol. 2010; 36:840–52. [PubMed: 20420973]

Vlachos F, Tung YS, Konofagou EE. Permeability assessment of the focused ultrasound-induced blood–brain barrier opening using dynamic contrast-enhanced MRI. Phys. Med. Biol. 2010; 55:5451–66. [PubMed: 20736501]

Xie F, Boska MD, Lof J, Uberti MG, Tsutsui JM, Porter TR. Effects of transcranial ultrasound and intravenous microbubbles on blood-brain barrier permeability in a large animal model. Ultrasound Med. Biol. 2008; 34:2028–34. [PubMed: 18692294]

Zheng H, Dayton PA, Caskey C, Zhao S, Qin S, Ferrara KW. Ultrasound-driven microbubble oscillation and translation within small phantom vessels. Ultrasound Med. Biol. 2007; 33:1978–87. [PubMed: 17900793]

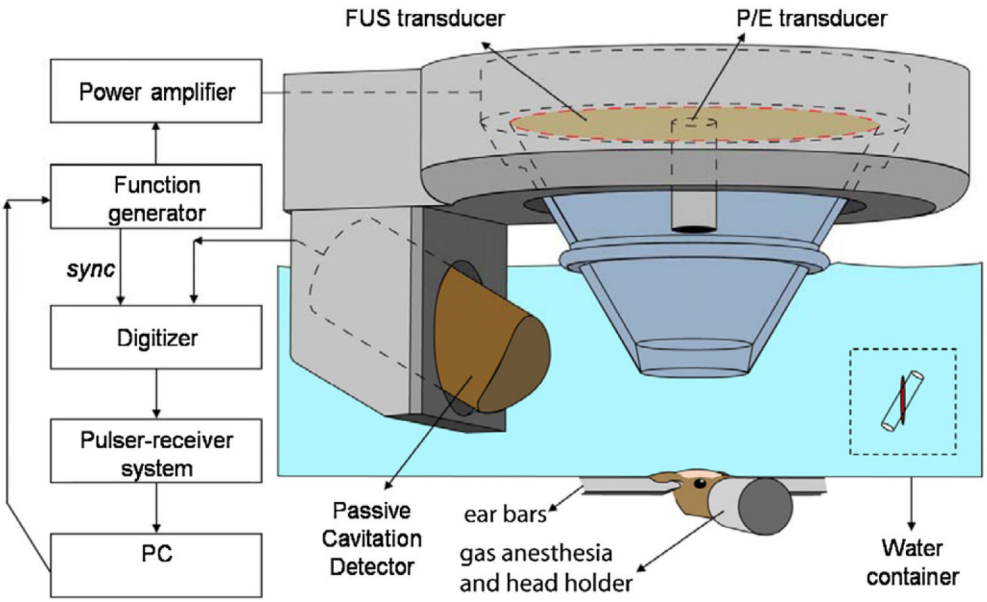

Figure 1.

Block diagram of the experimental setup. The PCD was positioned at 60° relative to the longitudinal axis of the FUS beam. The overlap between the focal regions of PCD (blue) and FUS (red) occurring inside the murine brain is illustrated in the inset.

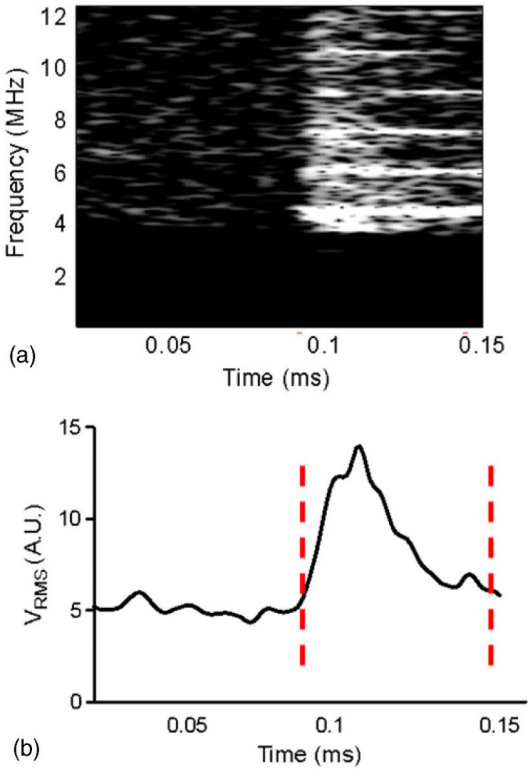

Figure 2.

Illustration of the ICD calculation of the *in vivo* experiments. (a) The spectrogram of the first pulse from 0.02 to 0.15 ms after a 4 MHz high-pass filter (Chebshev type 1) at 0.60 MPa. The harmonics and the broadband response could be observed in this figure. The corresponding V_{RMS} is depicted in (b) and the ICD was obtained using the integral of the V_{RMS} curve between two dashed lines.

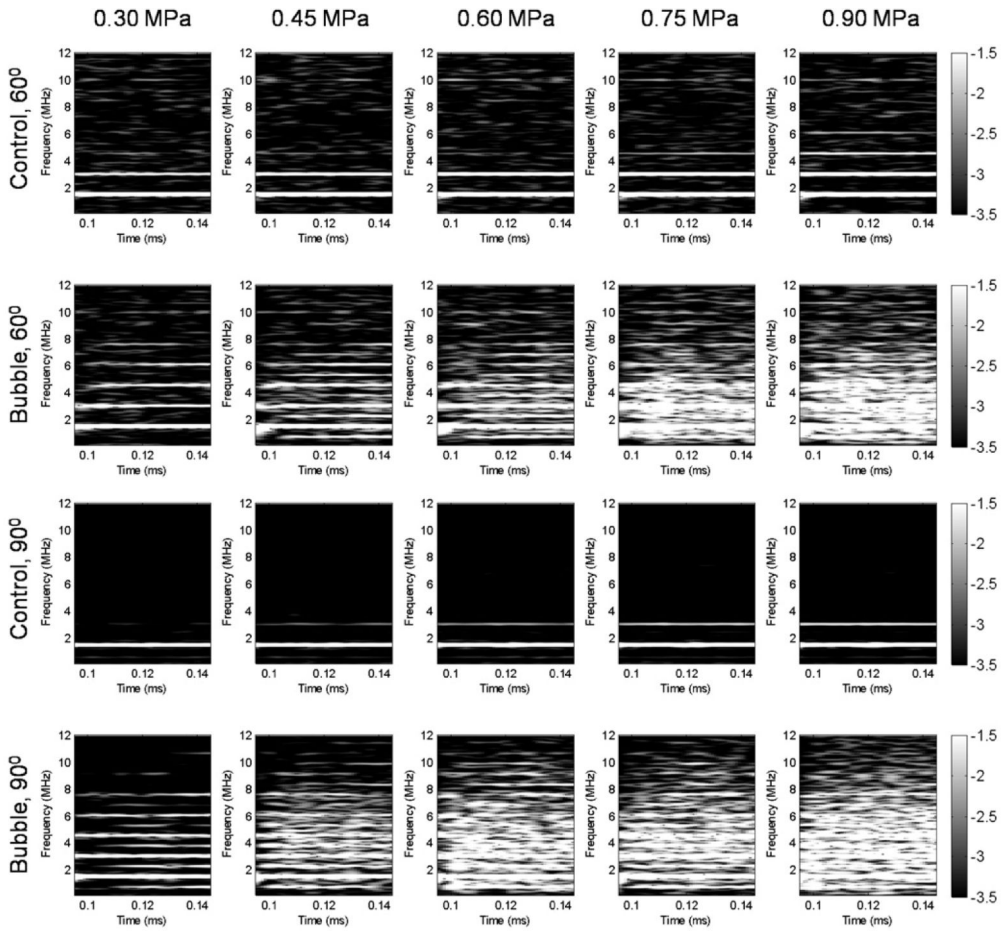

Figure 3.

Spectrogram of the first pulse in the phantom study without and with the microbubbles at five distinct acoustic pressures. Acoustic emissions were acquired with the hydrophone positioned at 60° and 90° from the longitudinal axis of the FUS beam. No broadband acoustic emissions were detected without the microbubbles while, with the microbubbles, the broadband acoustic emissions were detected at pressure equal to or higher than 0.45 MPa. At 0.30 MPa, the ultra-harmonics were detected at the 90° PCD but not at the 60° PCD.

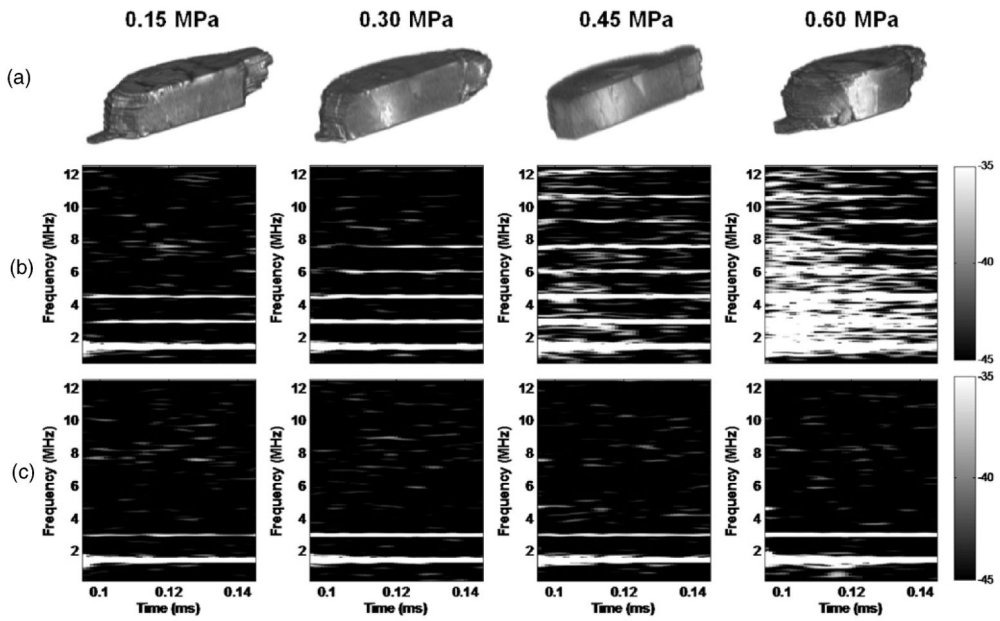

Figure 4.

BBB opening using transducer-A and microbubbles as confirmed by (a) 3D sagittal MRI and (b) the corresponding spectrogram (on the signal acquired by the hydrophone) of the first pulse from 0.095 to 0.145 ms showing that the broadband acoustic emissions were detected at 0.45 MPa and 0.60 MPa but not at 0.15 MPa and 0.30 MPa. 3D MR confirmed that BBB could open at 0.30 MPa, i.e. without inertial cavitation. (c) Spectrogram of the first pulse from 0.095 to 0.145 ms in the absence of microbubbles showing that only the first and second harmonics could be detected without microbubbles.

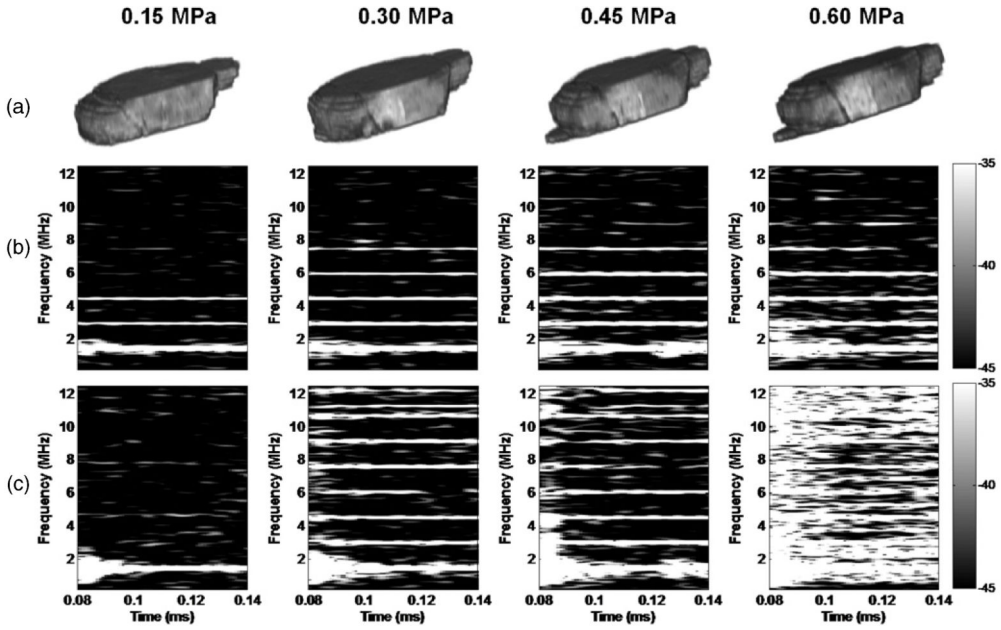

Figure 5.

BBB opening using transducer-B and microbubbles as confirmed by (a) 3D-MR images, and (b) the corresponding spectrogram (on the signal acquired by the hydrophone) of the first pulse from 0.095 to 0.145 ms showing that broadband acoustic emissions were detected at 0.45 MPa and 0.6 MPa but not at 0.15 MPa and 0.3 MPa. The 3D-MRI images confirmed that the BBB could open at 0.3 MPa, i.e. without inertial cavitation. (c) Spectrograms (on the signal acquired by the 10 MHz P/E transducer) also showed that the threshold of inertial cavitation was 0.45 MPa (see quantitative results in figure 6).

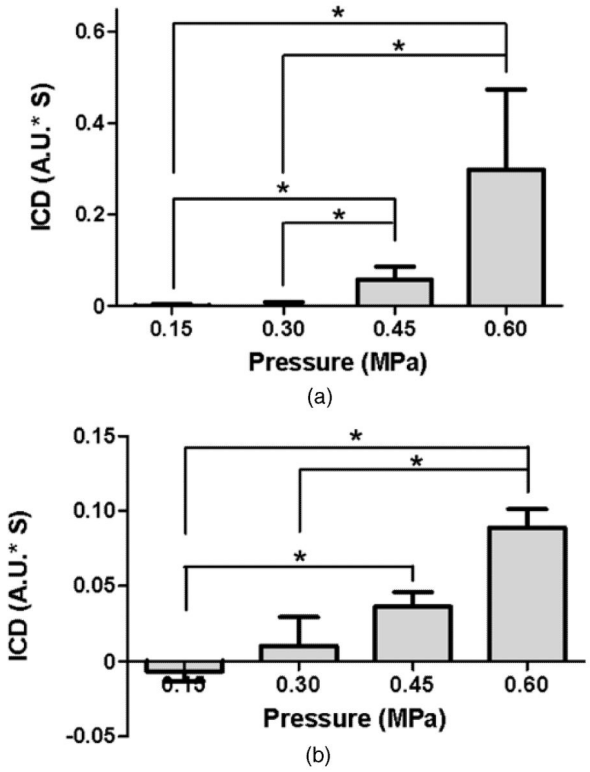

Figure 6.

ICD at four distinct acoustic pressures using (a) transducer-A or (b) transducer-B. ICD was quantified as the area under the V_{RMS} curve from 0.095 ms to 0.145 ms, at each pressure. The signal used for quantification was from a focused hydrophone. For transducer-A, the ICD at 0.45 MPa and 0.60 MPa was significantly higher than at 0.15 MPa and 0.30 MPa (*$P < 0.05$). For transducer-B, the ICD at 0.60 MPa was significantly higher than at 0.30 MPa and 0.15 MPa. The ICD at 0.45 MPa was also significantly higher than 0.15 MPa (* denotes $P < 0.05$).

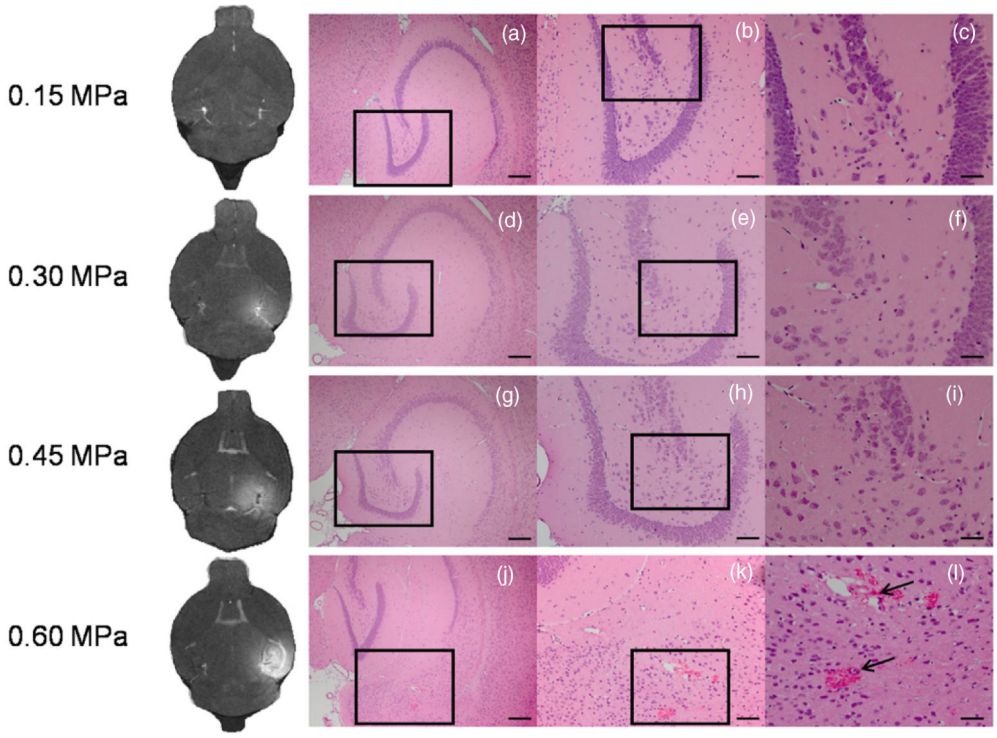

Figure 7.

2D-MRI images and H&E-stained horizontal sections of the BBB-opened hippocampi at (a-c) 0.15 MPa, (d-f) 0.30 MPa, (g-i) 0.45 MPa and (j-l) 0.60 MPa using transducer-A and microbubbles. Sonicated brains at 0.15 MPa, 0.30 MPa and 0.45 MPa showed no histological damage. Brain samples sonicated at 0.60 MPa (j)-(l) showed higher incidence of microscopic damage at multiple distinct damaged sites. The black arrows point to the RBC extravasations. The black boxes in the left and middle columns indicate the enlarged regions shown in the middle column and right column, respectively. Magnifications and scale bars in (a), (d), (g) and (j) are 40× and 200 μm, in (b), (e), (h) and (k) 100× and 100 μm and in (c), (f), (i) and (l) 200× and 50 μm, respectively.

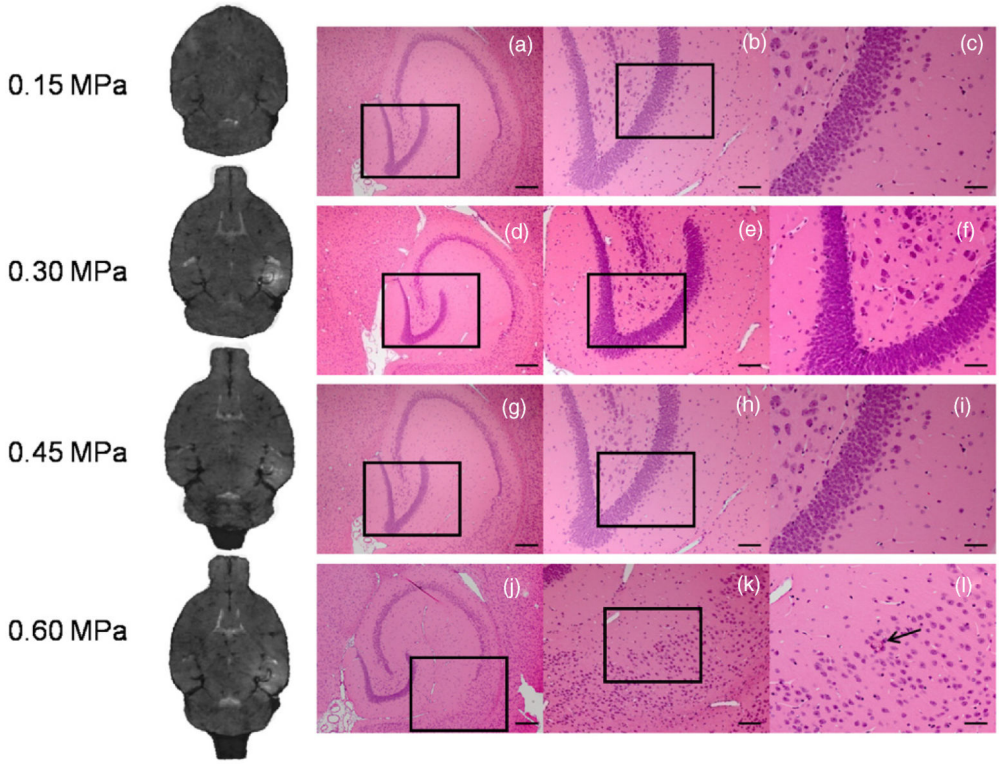

Figure 8.

2D-MR images and H&E-stained horizontal sections of the BBB-opened hippocampi at (a-c) 0.15 MPa, (d-f) 0.30 MPa, (g-i) 0.45 MPa and (j-l) 0.60 MPa using transducer-B and microbubbles. Sonicated brains at 0.15 MPa, 0.30 MPa and 0.45 MPa showed no histological damage. Minor microscopic damage was noticeable in one location of the right hippocampus sonicated at 0.60 MPa, constituting one distinct damaged site (g)-(i). Black arrows point to RBC extravasations. The black boxes inside the left and middle column show enlarged regions in the middle and right columns, respectively. Magnifications and scale bars in (a), (d), (g) and (j) are 40× and 200 μm, in (b), (e), (h) and (k) 100× and 100 μm and in (c), (f), (i) and (l) 200× and 50 μm, respectively.

Table 1

Number of mice with BBB opening/number of mice studied at each pressure.

	Pressure				
Transducer/PCD	**0.15 MPa**	**0.30 MPa**	**0.45 MPa**	**0.60 MPa**	**Total**
A/hydrophone	0/2	3/3	3/3	3/3	11
B/hydrophone	0/2	3/3	3/3	3/3	11
B/10 MHz P/E	0/1	1/1	1/1	1/1	4